iScience

CellPress

Article

Ultra-high Areal Capacity Realized in Three-Dimensional Holey Graphene/SnO_2 Composite Anodes

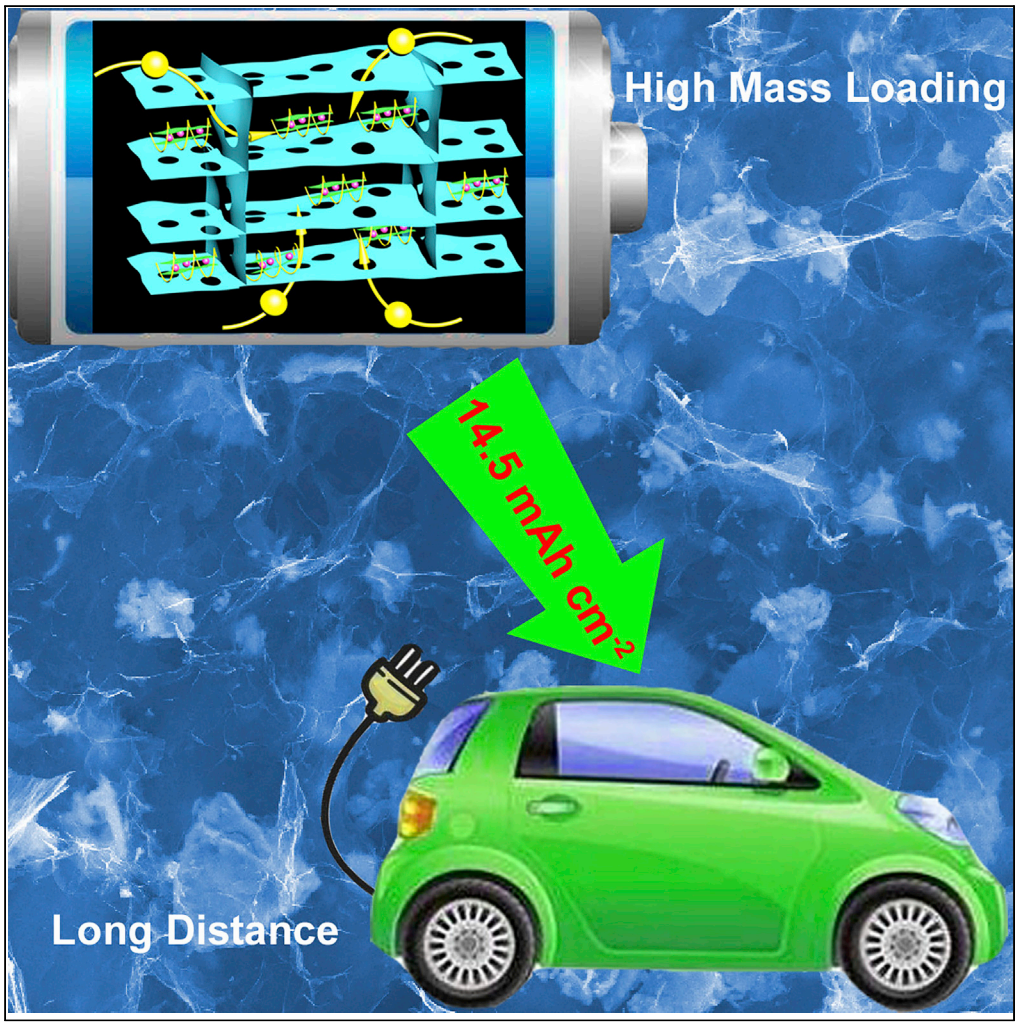

Junfei Liang, Hongtao Sun, Zipeng Zhao, ..., Lin Guo, Yu Huang, Xiangfeng Duan

linguo@buaa.edu.cn (L.G.)
yhuang@seas.ucla.edu (Y.H.)
xduan@chem.ucla.edu (X.D.)

HIGHLIGHTS

3D holey graphene framework/SnO_2 composite electrode was designed and prepared

Micrometer-sized SnO_2/graphene was impregnated into 3D holey graphene frameworks

The 3D composite anode can deliver an ultra-high areal capacity up to 14.5 mAh cm^{-2}

This study defines a critical step in exploring the alloy-type electrode for LIBs

Liang et al., iScience 19, 728–736
September 27, 2019
https://doi.org/10.1016/j.isci.2019.08.025

iScience

CellPress

Article

Ultra-high Areal Capacity Realized in Three-Dimensional Holey Graphene/SnO_2 Composite Anodes

Junfei Liang,[1,2,3,8] Hongtao Sun,[2,4,8] Zipeng Zhao,[1] Yiliu Wang,[2] Zhiying Feng,[2] Jian Zhu,[2,5] Lin Guo,[6,*] Yu Huang,[1,7,*] and Xiangfeng Duan[2,7,9,*]

SUMMARY

Nanostructured alloy-type electrode materials and its composites have shown extraordinary promise for lithium-ion batteries (LIBs) with exceptional gravimetric capacity. However, studies to date are usually limited to laboratory cells with too low mass loading (and thus too low areal capacity) to exert significant practical impact. Herein, by impregnating micrometer-sized SnO_2/graphene composites into 3D holey graphene frameworks (HGF), we show that a well-designed 3D-HGF/SnO_2 composite anode with a high mass loading of 12 mg cm^{-2} can deliver an ultra-high areal capacity up to 14.5 mAh cm^{-2} under current density of 0.2 mA cm^{-2} and stable areal capacity of 9.5 mAh cm^{-2} under current density of 2.4 mA cm^{-2}, considerably outperforming those in the state-of-art research devices or commercial devices. This robust realization of high areal capacity defines a critical step to capturing the full potential of high-capacity alloy-type electrode materials in practical LIBs.

INTRODUCTION

The development of advanced lithium-ion batteries (LIBs) with high energy density and long cycle life is critical for improving user experience with portable electronic devices and meeting the insatiable demands from electric vehicles and grid-level energy storage (Armand and Tarascon, 2008; Dunn et al., 2011; Lukatskaya et al., 2016). Alloy-type anode materials have attracted considerable interest as potential alternatives to state-of-the-art graphite anode for high-energy-density LIBs for their much higher theoretical capacity (e.g., 4,200 mAh g^{-1} in Si:; 990 mAh g^{-1} in Sn:; and 782 mAh g^{-1} in SnO_2: versus 372 mAh g^{-1} in graphite) (Idota et al., 1997; Qiu et al., 2010; Zhu et al., 2016). Despite enormous interest, the practical potential of such alloy-type anodes remains to be demonstrated to date. The extraordinary promise of such alloy-type anode is usually only achieved in research devices with relatively low mass loadings of the active materials (~1 mg cm^{-2}) and rather low areal capacity rarely exceeding those of today's LIBs (~3 mAh cm^{-2}) (Gallaghera et al., 2016). With such a low mass loading, the highly promising electrochemical performance achieved diminishes in practical devices when mass of the passive components such as current collectors and separators (e.g., ~5–10 mg cm^{-2}) is included (Cheng and Li, 2017; Gogotsi and Simon, 2011; Jin et al., 2017; Li et al., 2018; Liu et al., 2019; Mo et al., 2019; Sun et al., 2019). To fully capture the potential of such alloy-type anodes to impact practical technologies, it is imperative to considerably increase the areal mass loading to be at least comparable to that of the passive components and to achieve greatly higher areal capacity than that of the state-of-art devices today.

To increase the areal capacity by increasing the areal mass loading appears straightforward, but has met with limited success to date owing to a number of key challenges associated with the intrinsic nature of the alloy-type materials. First, the alloy-type anodes typically exhibit a large volume change upon lithiation and delithiation process (e.g., 400% for Si and 300% for SnO_2), which could lead to rapid pulverization during the charge/discharge process (Oumellal et al., 2011). Although this problem could be partially mitigated by various nanostructuring or compositing strategies (Huang et al., 2012; Li et al., 2016; Liu et al., 2014; Shi et al., 2018; Wang et al., 2013, 2016; Wu et al., 2012a, 2012b; Xia et al., 2016; Zhang et al., 2013), they are usually only applicable for electrodes with relatively low mass loading (<1 mg cm^{-2}). The volume change issue rapidly aggravates in thicker electrode at higher mass loading. The large volume swing between the charged and the discharged states results in excessive mechanical strain in the thicker electrode, leading to mechanical disintegration of the entire electrode structures and thus rapidly degrading cycling performance. Second, with their intrinsically high capacity, fully satisfying the charge storage capacity of

[1]Department of Materials Science and Engineering, University of California, Los Angeles, CA 90095, USA

[2]Department of Chemistry and Biochemistry, University of California, Los Angeles, CA 90095, USA

[3]School of Energy and Power Engineering, North University of China, Shanxi, Taiyuan 030051, P. R. China

[4]Department of Industrial and Manufacturing Engineering, The Pennsylvania State University, University Park, PA 16802-4400, USA

[5]College of Chemistry and Chemical Engineering, Hunan University, Changsha 410082, China

[6]School of Chemistry, Beihang University, Beijing 100191, China

[7]California NanoSystems Institute, University of California, Los Angeles, CA 90095, USA

[8]These authors contributed equally

[9]Lead Contact

*Correspondence: linguo@buaa.edu.cn (L.G.), yhuang@seas.ucla.edu (Y.H.), xduan@chem.ucla.edu (X.D.)

https://doi.org/10.1016/j.isci.2019.08.025

the thicker electrode requires delivery of substantially more charge (electrons and ions) into the electrode in a given area. In particular, such a requirement becomes increasingly more challenging in thicker electrode with higher mass loading, because a proportionally larger number of charges have to travel across a proportionally longer distance to fully utilize all the storage capacity of the active material in the thick electrode. Such a charge delivery requirement far exceeds that of typical electrode architecture design of the state-of-art batteries, posing a serious charge delivery challenge in fully utilizing the charge storage potential of such high-capacity materials at high mass loading. For the above challenges, the capacity and cycling performance rapidly degrade in electrode with the mass loading approaching practical levels ($\sim$10 mg cm^{-2}). Thus the alloy type anodes have exerted rather limited impact in practical technologies to date despite their extraordinary potential.

Here we report the design and preparation of 3D holey graphene framework/SnO_2 (3D-HGF/SnO_2) composite with ultra-high areal mass loading and ultra-high areal capacity. By impregnating the micrometer-sized SnO_2/graphene composites into the 3D-HGF, we produce a freestanding monolithic mechanical strong framework structure with interpenetrating electron transport and ion transport paths. Within such structure, the ultrasmall SnO_2 nanoparticles are fully embedded into the micrometer-sized composites and the graphene sheets can function as an effective encapsulation and buffer layer to accommodate the volume expansion of SnO_2 nanoparticles during lithiation process. The fully conjugated monolithic 3D graphene framework structure offers sufficient porosity, extraordinary mechanical strength, and mechanical flexibility to accommodate the large volume change of the alloy-type anode and ensure cycling durability. At the same time, the 3D-HGF structure also offers a fully conjugated graphene network for excellent electron conduction and fully interconnected hierarchical porous structure for ion transport, thus satisfying the charge delivery demand of the high-capacity alloy-type anodes, promising high utilization efficiency of the active material at practical levels of mass loading (Sun et al., 2017; Xu et al., 2014). We show that 3D-HGF/SnO_2 electrode with high mass loading up to 12 mg cm^{-2} can be created with ultra-high areal capacity up to 14.5 mAh cm^{-2} under current density of 0.2 mA cm^{-2} and stable areal capacity of 9.5 mAh cm^{-2} under current density of 2.4 mA cm^{-2}, considerably outperforming those in the state-of-the-art research devices or commercial devices. This work represents a critical step toward capturing the full potential of high-capacity alloy-type electrode materials in practical devices.

RESULTS

The freestanding 3D-HGF/SnO_2 composites were prepared using a two-step process. In the first step, the SnO_2 nanoparticles were directly grown on freestanding graphene sheets through a hydrothermal process followed by a freeze-drying process and then an annealing at 500°C to obtain micrometer-sized SnO_2/G composites. The SnO_2/G composites were then mixed with holey graphene oxide sheets and conjugated into a freestanding 3D framework structure using ascorbate reduction process (Figure 1A), which was then freeze-dried and annealed at 500°C under argon flow for 2 h to produce freestanding monolithic 3D porous composites with the HGF as the conductive scaffolds for micrometer-sized SnO_2/graphene composites (Figure 1B). Within such composite, the SnO_2 nanoparticles are fully buried into the micrometer-sized composites and the graphene sheets can act as cushion to accommodate the volume expansion of SnO_2 nanoparticles during lithiation process. The micrometer-sized SnO_2/graphene composites were impregnated into 3D HGF, which can offer an effective encapsulation and buffer layer to further accommodate the volume changes and ensure cycling durability. Meanwhile, the 3D HGF also provides rapid interpenetrating pathways for both electrons and ions and sustains high utilization efficiency of the active material at high mass loading levels.

SnO_2 nanoparticles can interact with graphene sheets through physisorption and electrostatic binding. In addition, the residue oxygenic groups on the reduced graphene oxide could also chemically bind to SnO_2 nanoparticles (Wu et al., 2012a, 2012b). The transmission electron microscopic (TEM) image clearly reveals well-distributed SnO_2 nanoparticles decorated on the graphene sheets with average size of around 5–8 nm (Figure 1C). The lattice-resolved TEM image shows a lattice spacing of 0.33 nm (Figure 1D), corresponding to the (110) plane of the SnO_2. The X-ray diffraction studies of the freestanding HGF/SnO_2 composite show consistent diffraction pattern matching well with the standard SnO_2 card (JCPDS no. 41-1445), indicating the high purity of the SnO_2 in the composites (Figure 1E). Based on the diffraction peak width, we can also determine the average particle size to be $\sim$8 nm using Sherrer's formula, consistent with TEM studies. The small particle size is beneficial for withstanding volume expansion or contraction during the charge/discharge processes and improving capacity and rate performance of 3D HGF/SnO_2 by shortening the Li^+ diffusion distance in Li_xSnO_2 (Xia et al., 2016). Raman spectroscopy studies show the expected D and

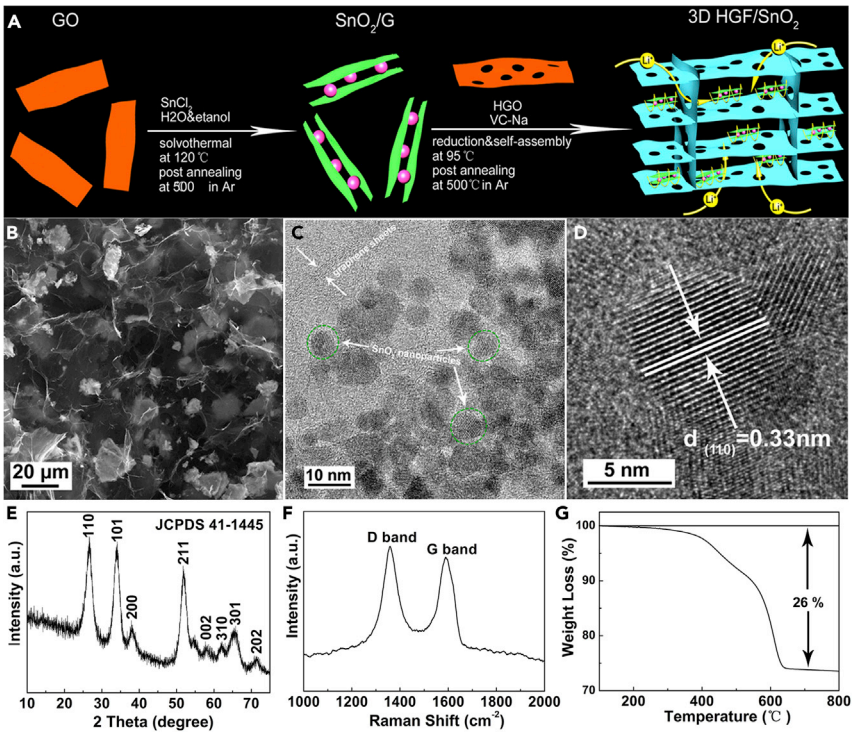

Figure 1. Preparation and Characterization of 3D HGF/SnO_2

(A) Schematic illustration of preparation of 3D HGF/SnO_2.

(B) Cross-sectional scanning electron microscopic image shows interior microstructures of HGF/SnO_2. The SnO_2 nanoparticles were first grown on graphene sheets to obtain micrometer-sized SnO_2/G composites, which were then incorporated into a 3D HGF to form the composite anode.

(C) TEM image of graphene sheets with uniformly decorated SnO_2 nanoparticles.

(D) High-resolution TEM image of SnO_2 nanoparticles.

(E) X-ray diffraction patterns of the as-synthesized freestanding HGF/SnO_2 composite.

(F) Raman spectra of HGF/SnO_2 electrodes. The D and G bands are characteristic of RGO.

(G) Thermogravimetric analysis of HGF/SnO_2 electrodes.

G bands of reduced GO (RGO) in the composites (Figure 1F). Thermogravimetric analysis shows a clear mass loss at 600°C, indicating that the mass percentage of RGO in the as-prepared HGF/SnO_2 composite is 26% (Figure 1G). Together, these structural analyses clearly demonstrate that the two-step synthesis effectively produces mechanically strong 3D porous composites with a high loading of SnO_2 nanoparticles.

We have next tested the Li storage performance of 3D-HGF/SnO_2 composites at different mass loadings. As a control sample, the simple G/SnO_2 slurry composite with a randomly stacked graphene network (the synthesis processes are described in the Supplemental Information) was also prepared and compared. Electrodes with three different levels of mass loading were investigated, corresponding to a typical loading amount for research studies (2 mg cm^{-2}), one that is representative of practical levels of mass loading (12 mg cm^{-2}) and an intermediate level of mass loading (7 mg cm^{-2}). For the G/SnO_2 control electrodes, it is apparent that galvanostatic charge/discharge characteristics vary dramatically at different mass loadings (Figure 2A). The voltage-capacity curves exhibit an increasingly steeper slope and larger voltage drop at higher mass loading, with rapidly degrading gravimetric capacity within a given potential window, which can be attributed to an increasingly larger internal resistance in thicker electrode, which in turn leads to higher overpotentials and lower capacities (Singh et al., 2015). In contrast, the charge/discharge curves of the 3D-HGF/SnO_2 electrodes show a relatively small voltage drop and capacity loss with increasing mass loading (Figure 2B), indicating that HGF/SnO_2 exhibits much smaller overpotential, which might be largely attributed to the much smaller internal resistance of the 3D-HGF composite structure. As a result, the HGF/SnO_2 electrode shows much less capacity degradation induced by mass loading at various C-rates. In contrast, increased mass loading for G/SnO_2 control electrodes leads to a significant decrease

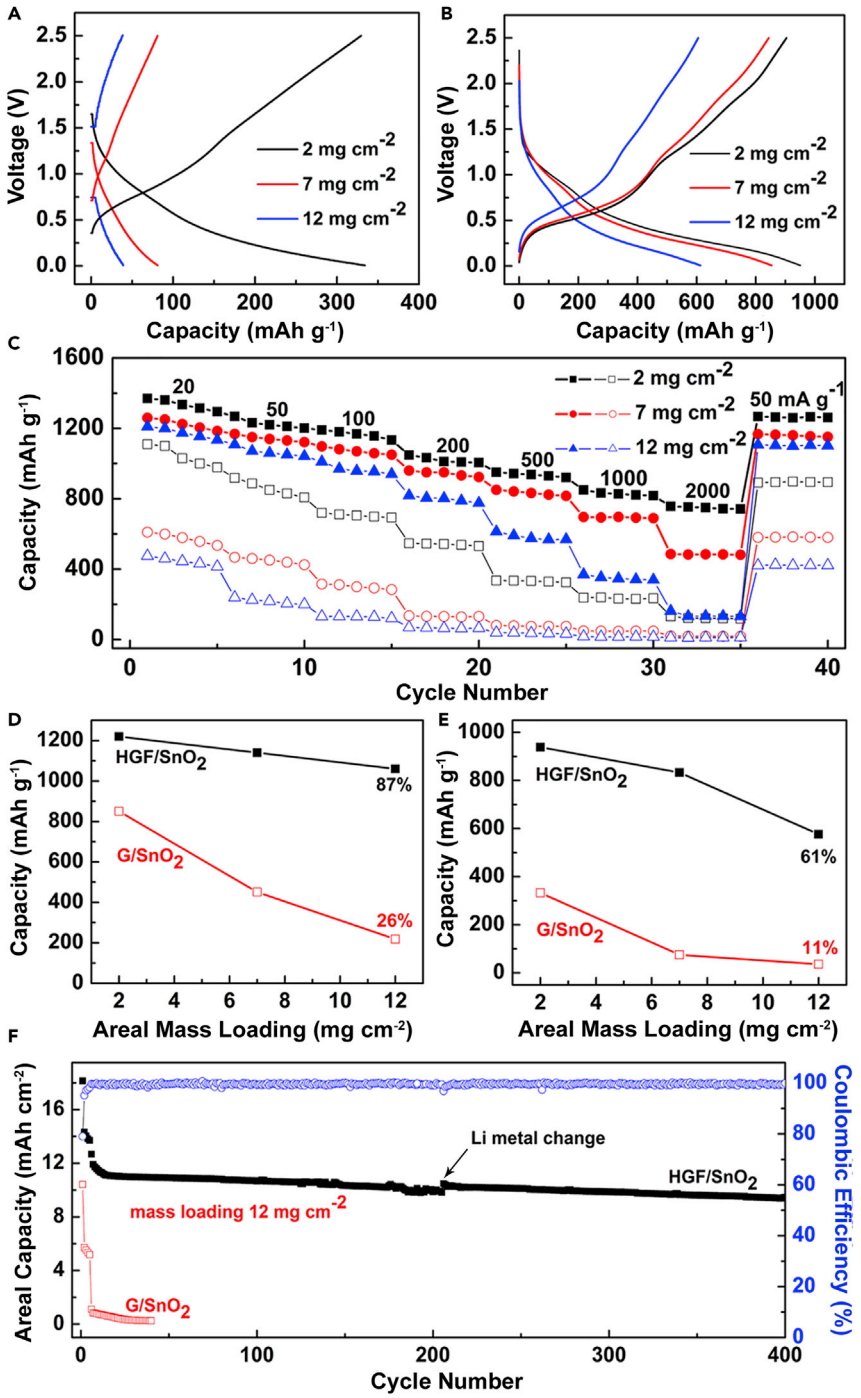

Figure 2. Effects of Mass Loading on Electrochemical Characteristics

(A and B) Galvanostatic charge/discharge curves for (A) the G/SnO_2 control electrode and (B) the HGF/SnO_2 electrode at a current density of 500 mA g^{-1} for mass loadings of 2, 7, and 12 mg cm^{-2}.

(C) Comparison of the rate performance between 20 mA g^{-1} and 2,000 mA g^{-1} for HGF/SnO_2 (solid) and G/SnO_2 (open) electrodes under different mass loadings (2, 7, and 12 mg cm^{-2}).

(D and E) Retention of specific capacity of HGF/SnO_2 (solid) and G/SnO_2 (open) anodes at (D) 50 mA g^{-1} and (E) 500 mA g^{-1} with increasing mass loadings.

Figure 2. *Continued*

(F) The cycle performance of HGF/SnO_2 and G/SnO_2 electrode with mass loading of 12 mg cm^{-2} at a current density of 2.4 mA cm^{-2}. The Li metal counterelectrode was replaced at the 206th cycle to avoid impact by the degradation of the Li metal electrode. The electrochemical properties were normalized by the total mass of the electrode materials (HGF/SnO_2 electrodes free of conductive additives and binders and the control G/SnO_2 including binders and conductive additives).

in energy storage properties with essentially diminished capacity at high C-rate (e.g., >500 mA cm^{-2}) (Figures 2C and S1).

These studies at different C-rates further demonstrate exceptional capability of HGF/SnO_2 to retain high capacitance at high mass loading at various current densities. For example, a capacity of 1,060 mAh g^{-1} is maintained in electrode with 12 mg cm^{-2} loading at a current density of 50 mA g^{-1}, which is only 13% less than that (1,220 mAh g^{-1}) with 2 mg cm^{-2} mass loading (Figure 2D). Even at the high current of 500 mA g^{-1}, the HGF/SnO_2 electrode retains a capacity of 576 mAh g^{-1} at a mass loading of 12 mg cm^{-2}, a 39% decrease of from 938 mAh g^{-1} at the 2-mg cm^{-2} electrode (Figure 2E). In contrast, in the G/SnO_2 electrodes, the gravimetric capacity seriously degraded from 850 to 218 mAh g^{-1} when the mass loading is increased from 2 mg cm^{-2} to 12 mg cm^{-2} at a current density of 50 mA g^{-1}; at higher current density of 500 mA g^{-1}, even more severe decrease in energy storage properties is observed in high mass loading electrodes with only 36 mAh g^{-1} left in electrode with 12 mg cm^{-2} mass loading (Figure 2D). Such a large degradation in performance with increasing mass loading highlights the challenges in delivering sufficient ionic current densities to retain the same gravimetric energy storage performance in thicker electrodes.

The encapsulation of the SnO_2 nanoparticles in SnO_2/graphene composites and then impregnation of the micrometer-sized composites into strong 3D-HGF offers sufficient flexibility and space to accommodate the repeated volume change during the charge/discharge process to ensure excellent cycling stability at high mass loading. To this end, we have tested the cycling stability of 3D-HGF/SnO_2 electrodes and compared against that of G/SnO_2 electrode at a mass loading of 12 mg cm^{-2} (Figure 2F). Under a current density of 2.4 mA cm^{-2}, the reversible capacity of the HGF/SnO_2 electrodes can be as high as 9.5 mA h cm^{-2} after 400 cycles, with the Coulombic efficiency consistently above 99.9%, demonstrating the robust porous architecture of the 3D composites. In contrast, the G/SnO_2 electrode exhibited a very poor cycling performance, with a rapid fading of capacity to 0.25 mAh cm^{-2} after 40 cycles owing to the severe pulverization. In this work, we impregnated micrometer-sized SnO_2/graphene composites as a secondary structure into 3D HGF, so the solid-electrolyte interface largely forms the outer layer of the secondary structure, which makes the whole structure more static during charge/discharge processes. Compared with the control G/SnO_2 electrode without secondary microstructure, our electrode showed considerably higher first cycle Coulombic efficiency of 79.2% (55.1% for the control electrode) and more stable cycling performance. It should be noted that, at such high areal capacity and current density, the stability of Li-metal electrode poses a challenge for long cycling durability test. To this end, we have replaced the Li metal counterelectrode with a fresh one at the 206th cycle so that the degradation of the Li metal counterelectrode would not affect the cycling performance of the HGF/SnO_2 electrodes.

The ability to retain high electrochemical performance and achieve high areal capacity at high mass loading is critical for practical applications, because a higher mass loading can reduce the relative overhead from the current collectors and separators and is thus critical for achieving higher cell-level energy density (Gallaghera et al., 2016). For this reason, the areal capacity provides an important measure for assessing the practical performance of electrode materials for LIBs (Singh et al., 2015). To this end, we have evaluated the areal capacity (mAh cm^{-2}) as a function of areal mass loading (mg cm^{-2}).

In the ideal case, the areal capacity scales proportionally with increasing mass loading of the active materials. However, owing to charge transport limitations, a sublinear relationship or inverse relationship can be observed in many electrode materials. For example, for the G/SnO_2 electrodes, the areal capacity only increased by 53% from 1.44 to 2.21 mAh cm^{-2}, when the mass loading is increased by 250% from 2 to 7 mg cm^{-2}. Even worse, when the mass loading is further increased to 12 mg cm^{-2}, the areal capacity is decreased to 1.57 mAh cm^{-2}, which can be attributed to reducing the utilization efficiency of the active materials with increasing charge transport resistance in thicker electrode. On the other hand, for 3D-HGF/SnO_2 composite with optimized charge transport properties, a nearly linear scaling relationship is observed. When the mass loading is increased from 2 to 7 mg cm^{-2}, the areal capacity is nearly proportionally increased from 2.38 to 7.68 mAh cm^{-2}, indicating no charge transport limitation in these mass

loading ranges. With further increase in the mass loading to 12 mg cm^{-2}, the areal mass loading is further increased to 12.13 mAh cm^{-2} (Figure 3A). Apparently, the areal capacity increase slows at higher mass loading, suggesting that the charge transport resistance starts to play a limiting role in such a thick electrode.

We have further evaluated the areal capacity versus areal mass loading for the HGF/SnO_2 composite electrode at different current densities (Figure 3B). At relatively low current densities of 20, 50, and 100 mA g^{-1}, the areal capacity increases linearly with mass loading until 12 mg cm^{-2}. At higher current density beyond 500 mA g^{-1}, the areal capacity starts to deviate from linearity to reach a plateau at a high mass loading of 12 mg cm^{-2}. The plateau-like behavior indicates that the penetration depth limit for the ionic current has been reached at such current density, as previously suggested by Gallagher et al. (Gallaghera et al., 2016). The transition between the linear response and the plateau suggests that the higher loading becomes progressively less beneficial, particularly at higher current density regime.

At even higher current density of 1,000 mA g^{-1}, the areal capacity experiences a slight decrease at high mass loading, suggesting that the charge transport resistance starts to limit the utilization efficiency of the active materials at such high rate. The decrease in areal capacity (for example, 1,000 mA g^{-1} at loadings of 12 mg cm^{-2}) can be attributed to concentration polarization due to insufficient charge (ion) delivery rate to fully satisfy the charge storage requirements (Sun et al., 2017).

To further evaluate the Li storage performance at different current densities and probe the charge delivery limitations, we have plotted the areal capacity as a function of areal current density for the 3D-HGF/SnO_2 electrodes at different mass loadings (Figure 3C). At low-enough current density, the areal capacities level off near the maximum theoretical value as all the electrode material becomes accessible to electrolyte penetration and can be fully utilized when the charge and discharge rates are sufficiently slow. Notably, in this regard, a maximum areal capacity of 14.5 mAh cm^{-2} is reached at mass loading of 12 mg cm^{-2}, considerably higher than the areal capacity achieved with the previous anode materials and structures. It is also noted that all the electrode with different mass loadings show a rapid decrease in areal capacity when the current density is increased beyond 10 mA cm^{-2}, suggesting that charge transport within the electrolyte is becoming the limiting factor at such current density (Gallaghera et al., 2016). It is also interesting to note that such a decrease in capacity around 10 mA cm^{-2} also coincides with a similar decrease observed in 3D-HGF/Nb_2O_5 composites at similar current densities. Such a collapse at a similar critical current density indicates that a similar ion delivery limitation is achieved with these different 3D-HGF composite materials, which might be attributed to an intrinsic ion diffusion limitation of the 3D-HGF structures.

We have also compared the areal capacity versus current density with those of the state-of-the-art commercial graphite anodes (Billaud et al., 2016; Gallaghera et al., 2016; Moshtev and Johnson, 2000) and representative research anodes (such as Si and SnO_2) (Figure 4A) (Cui et al., 2009; Jahel et al., 2014; Li et al., 2014; Oumellal et al., 2011; Shi et al., 2018; Wu et al., 2012a, 2012b; Zhang et al., 2016; Zhou et al., 2016). Compared with typical commercial or research devices, our composite electrode delivers a much higher areal capacity at a given current density, almost doubling the highest value reported before. It is noted that the areal capacity achieved in HGF/SnO_2 is lower than that of the previously reported Nb_2O_5/HGF electrode under ultra-high current of 20 mA cm^{-2}, at which regime the charge transport might be limited, relatively slower Li^+ ion diffusion inside SnO_2 when compared with much faster diffusion in Nb_2O_5. The superior performance of HGF/SnO_2 is more evident in the linear plot of the areal capacity versus current density (Figure S2). The advantage of having electrodes with high mass loading becomes more apparent when the mass of the inactive components (such as current collectors ~10 mg cm^{-2}) is taken into account (Gogotsi and Simon, 2011; Singh et al., 2015). For example, normalizing the capacity by the mass of the entire electrode (including the electrode materials and the current collector) the 3D HGF/SnO_2 electrode delivers highest specific electrode capacity when the current density is less than 500 mA g^{-1} (almost doubling the previous record) (Figure 4B).

DISCUSSION

Together, we have demonstrated that a freestanding 3D-HGF/SnO_2 composite, in which the mechanically strong 3D-HGF offers sufficient space and flexibility to accommodate the volume expansion of SnO_2 nanoparticles while providing efficient electron and ion transport pathways, fully captures the merit of high-capacity alloy-type anode materials in high areal mass loading electrodes and achieves an extraordinary areal capacity up to 14.5 mAh cm^{-2}. We should note that although a high mass loading electrode has been

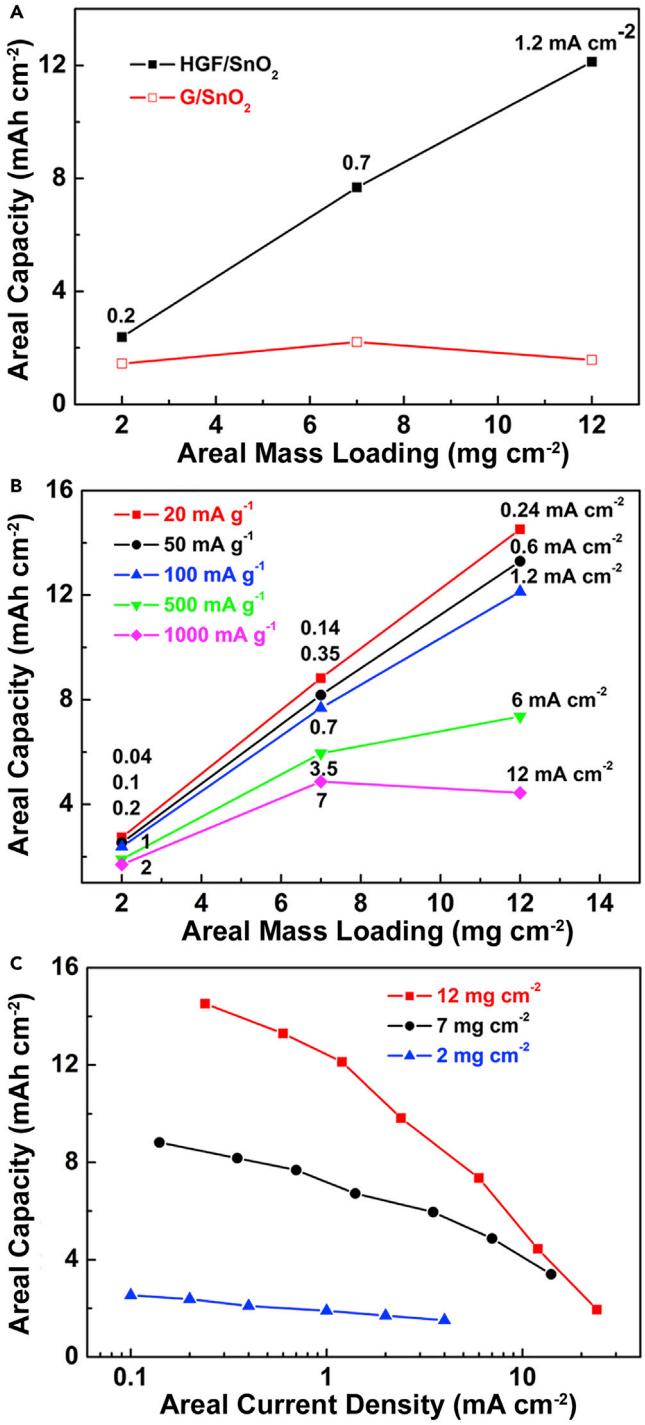

Figure 3. Performance Metrics for Electrodes with High Mass Loading

(A) Dependence of areal capacity on mass loading at 100 mA g^{-1} for HGF/SnO_2 and G/SnO_2 electrodes.

(B) The correlation of areal capacity with mass loading (2, 7, and 12 mg cm^{-2}) at various current densities for the HGF/SnO_2 electrode.

(C) The effect of current density and mass loading on the areal capacity of the HGF/SnO_2 electrode.

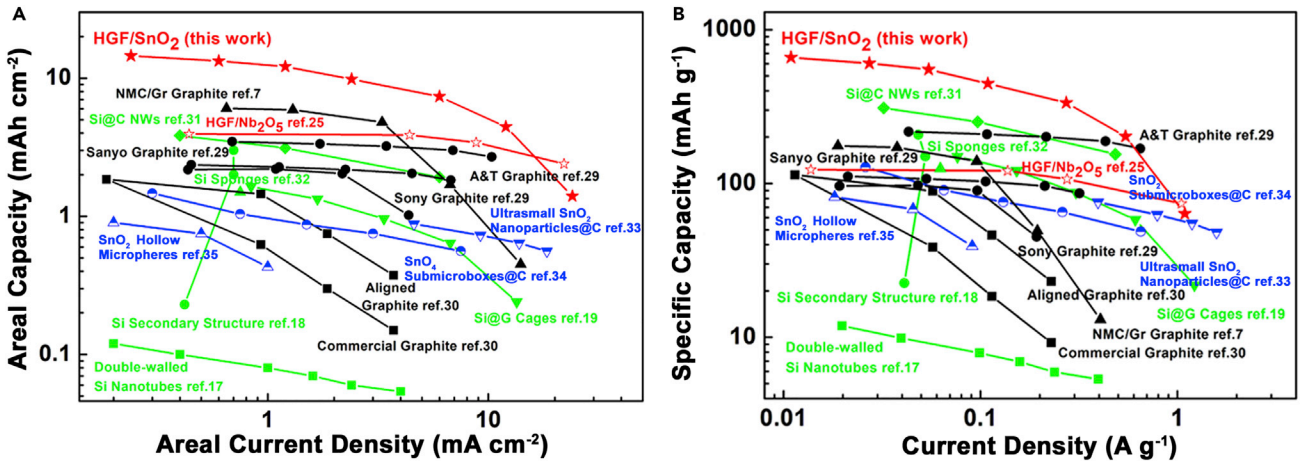

Figure 4. Comparison of Energy Storage Performance Metrics for Various Anode Materials

(A) Comparison of areal performance metrics of SnO_2/HGF electrode with those of various commercial and research anodes, including graphite anodes and high-capacity Si and SnO_2 anodes.

(B) Comparison of specific capacities at various current densities normalized by the total mass of the electrode (including the electrode materials, the current collector, and any other additives when applicable).

demonstrated as an ultra-high rate anode based on a similar 3D-HGF/Nb_2O_5 composite structure, the areal capacity achieved there is limited (~4 mAh cm^{-2}) owing to the intrinsically lower theoretical capacity of the Nb_2O_5 anode materials. It is important to note that the ultra-high areal capacity up to 14.5 mAh cm^{-2} achieved in the current study represents one of the highest areal capacities achieved in all anode materials reported to date, to the best of our knowledge. It is also worth noting that our HGF/SnO_2 electrode does not contain any other binder or conductive additive and shows the highest specific capacity reported to date when normalized by the total weight of the entire electrode (electrode composite materials and the current collector). This study thus defines a critical step in exploring the high-capacity alloy-type electrode materials for practical electrochemical energy storage devices.

Limitations of the Study

Although this solution-processable self-assembly approach shows great promise for large-scale production of 3D graphene-based composite electrodes, it is still a batch process that can limit the production throughput. To solve this issue, a scalable manufacturing process capable of high-throughput production (e.g., a roll-to-roll process) is highly desirable for practical battery manufacturing.

METHODS

All methods can be found in the accompanying Transparent Methods supplemental file.

SUPPLEMENTAL INFORMATION

Supplemental Information can be found online at https://doi.org/10.1016/j.isci.2019.08.025.

ACKNOWLEDGMENTS

X.D. acknowledges support from National Science Foundation Grant No. 1800580. Y.H. acknowledges partial support from Office of Naval Research grant N000141812155.

AUTHOR CONTRIBUTIONS

X.D., Y.H., and L.G. designed and supervised the research; J.L. synthesized the material; J.L. and H.S. conducted the characterization with assistance from Z.Z., Y.W., Z.F., and J.Z.; J.L. and H.S. analyzed the data and prepared the figures. X.D. and J.L. wrote the manuscript with input from all coauthors. All the authors participated in discussions of the research.

DECLARATION OF INTERESTS

The authors declare no competing interests.

Received: March 25, 2019
Revised: June 25, 2019
Accepted: August 13, 2019
Published: September 27, 2019

REFERENCES

Armand, M., and Tarascon, J.M. (2008). Building better batteries. Nature *451*, 652–657.

Billaud, J., Bouville, F., Magrini, T., Villevieille, C., and Studart, A.R. (2016). Magnetically aligned graphite electrodes for high-rate performance Li-ion batteries. Nat. Energy *1*, 16097.

Cheng, H.M., and Li, F. (2017). Charge delivery goes the distance. Science *356*, 581–582.

Cui, L.–F., Yang, Y., Hsu, C.–M., and Cui, Y. (2009). Carbon–silicon core–shell nanowires as high capacity electrode for lithium ion batteries. Nano Lett. *9*, 3370–3374.

Dunn, B., Kamath, H., and Tarascon, J.M. (2011). Electrical energy storage for the grid: a battery of choices. Science *334*, 928–935.

Gallaghera, K.G., Traska, S.E., Bauerb, C., Woehrleb, T., Luxc, S.F., Tschechb, M., Lampb, P., Polzina, B.J., Haa, S., Longa, B., et al. (2016). Optimizing areal capacities through understanding the limitations of lithium-ion electrodes. J. Electrochem. Soc. *163*, A138–A149.

Gogotsi, Y., and Simon, P. (2011). True performance metrics in electrochemical energy storage. Science *334*, 917–918.

Huang, X., Qi, X., Boeyab, F., and Zhang, H. (2012). Graphene-based composites. Chem. Soc. Rev. *41*, 666–686.

Idota, Y., Kubota, T., Matsufuji, A., Maekawa, Y., and Miyasaka, T. (1997). Tin-based amorphous oxide: a high-capacity lithium-ion-storage material. Science *276*, 1395–1397.

Jahel, A., Ghimbeu, C.M., Monconduit, L., and Vix-Guterl, C. (2014). Confined ultrasmall SnO_2 particles in micro/mesoporous carbon as an extremely long cycle-life anode material for Li-ion batteries. Adv. Energy Mater. *4*, 1400025.

Jin, S., Sun, Z., Guo, Y., Qi, Z., Guo, C., Kong, X., Zhu, Y., and Ji, H. (2017). High areal capacity and lithium utilization in anodes made of covalently connected graphite microtubes. Adv. Mater. *38*, 1700783.

Li, X., Gu, M., Hu, S., Kennard, R., Yan, P., Chen, X., Wang, C., Sailor, M.J., Zhang, J.G., and Liu, J. (2014). Mesoporous silicon sponge as an anti-pulverization structure for high-performance lithium-ion battery anodes. Nat. Commun. *5*, 4105.

Li, Y., Yan, K., Lee, H.-W., Lu, Z., Liu, N., and Cui, Y. (2016). Growth of conformal graphene cages on micrometre-sized silicon particles as stable battery anodes. Nat. Energy *1*, 15029.

Li, Z., He, Q., Xu, X., Zhao, Y., Liu, X., Zhou, C., Ai, D., Xia, L., and Mai, L. (2018). A 3D nitrogen-doped graphene/TiN nanowires composite as a strong polysulfide anchor for lithium-sulfur batteries with enhanced rate performance and high areal capacity. Adv. Mater. *45*, 1804089.

Liu, N., Lu, Z., Zhao, J., McDowell, M.T., Lee, H.-W., Zhao, W., and Cui, Y. (2014). A pomegranate-inspired nanoscale design for large-volume-change lithium battery anodes. Nat. Nanotechnol. *9*, 187–192.

Liu, T., Zhou, Z., Guo, Y., Guo, D., and Liu, G. (2019). Block copolymer derived uniform mesopores enable ultrafast electron and ion transport at high mass loadings. Nat. Commun. *10*, 675.

Lukatskaya, M.R., Dunn, B., and Gogotsi, Y. (2016). Multidimensional materials and device architectures for future hybrid energy storage. Nat. Commun. *7*, 12647.

Mo, R., Li, F., Tan, X., Xu, P., Tao, R., Shen, G., Lu, X., Liu, F., Shen, L., Xu, B., et al. (2019). High-quality mesoporous graphene particles as high-energy and fast-charging anodes for lithium-ion batteries. Nat. Commun. *10*, 1474.

Moshtev, R., and Johnson, B. (2000). State of the art of commercial Li ion batterials. J. Power Sources *91*, 86–91.

Oumellal, Y., Delpuech, N., Mazouzi, D., Dupré, N., Gaubicher, J., Moreau, P., Soudan, P., Lestriez, B., and Guyomard, D. (2011). The failure mechanism of nano-sized Si-based negative electrodes for lithium ion batteries. J. Mater. Chem. *21*, 6201–6208.

Qiu, Y., Yan, K., and Yang, S. (2010). Ultrafine tin nanocrystallites encapsulated in mesoporous carbon nanowires: scalable synthesis and excellent electrochemical properties for rechargeable lithium ion batteries. Chem. Commun. *46*, 8359–8361.

Shi, H., Fang, Z., Zhang, X., Li, F., Tang, Y., Zhou, Y., Wu, P., and Yu, G. (2018). Double-network nanostructured hydrogel-derived ultrafine Sn-Fe alloy in three-dimensional carbon framework for enhanced lithium storage. Nano Lett. *5*, 3193–3198.

Singh, M., Kaiser, J., and Hahn, H. (2015). Thick electrodes for high energy lithium ion batteries. J. Electrochem. Soc. *162*, A1196–A1201.

Sun, H., Mei, L., Liang, J., Zhao, Z., Lee, C., Fei, H., Ding, M., Lau, J., Li, M., Wang, C., et al. (2017). Three-dimensional holey-graphene/niobia composite architectures for ultrahigh-rate energy storage. Science *356*, 599–604.

Sun, H., Zhu, J., Baumann, D., Peng, L., Xu, Y., Shakir, I., Huang, Y., and Duan, X. (2019). Hierarchical 3D electrodes for electrochemical energy storage. Nat. Rev. Mater. *1*, 45–60.

Wang, D., Yang, J., Li, X., Geng, D., Li, R., Cai, M., Sham, T.K., and Sun, X. (2013). Layer by layer assembly of sandwiched graphene/SnO_2 nanorod/carbon nanostructures with ultrahigh lithium ion storage properties. Energy Environ. Sci. *6*, 2900–2906.

Wang, J., Tang, H., Zhang, L., Ren, H., Yu, R., Jin, Q., Qi, J., Mao, D., Yang, M., Wang, Y., et al. (2016). Multi-shelled metal oxides prepared via an anion-adsorption mechanism for lithium-ion batteries. Nat. Energy *1*, 16050.

Wu, H., Chan, G., Choi, J.W., Ryu, I., Yao, Y., McDowell, M.T., Lee, S.W., Jackson, A., Yang, Y., Hu, L., et al. (2012a). Stable cycling of double-walled silicon nanotube battery anodes through solid-electrolyte interphase control. Nat. Nanotechnol. *7*, 310–315.

Wu, Z.-S., Zhou, G., Yin, L.-C., Ren, W., Li, F., and Cheng, H.-M. (2012b). Graphene/metal oxide composite electrode materials for energy storage. Nano Energy *1*, 107–131.

Xia, L., Wang, S., Liu, G., Ding, L., Li, D., Wang, H., and Qiao, S. (2016). Flexible SnO_2/N-doped carbon nanofiber films as integrated electrodes for lithium-ion batteries with superior rate capacity and long cycle life. Small *7*, 853–859.

Xu, Y., Lin, Z., Zhong, X., Huang, X., Weiss, N.O., Huang, Y., and Duan, X. (2014). Holey graphene frameworks for highly efficient capacitive energy storage. Nat. Commun. *5*, 4554.

Zhang, J., Ren, H., Wang, J., Qi, J., Yu, R., Wang, D., and Liu, Y. (2016). Engineering of multi-shelled SnO_2 hollow microspheres for highly stable lithium-ion batteries. J. Mater. Chem. A *4*, 17673–17677.

Zhang, L., Zhang, G., Wu, H.B., Yu, L., and Lou, X.W. (2013). Hierarchical tubular structures constructed by carbon-coated SnO_2 nanoplates for highly reversible lithium storage. Adv. Mater. *25*, 2589–2593.

Zhou, X., Yu, L., and Lou, X.W. (2016). Formation of uniform N-doped carbon-coated SnO_2 submicroboxes with enhanced lithium storage properties. Adv. Energy Mater. *6*, 1600451.

Zhu, J., Shan, Y., Wang, T., Sun, H., Zhao, Z., Mei, L., Fan, Z., Xu, Z., Shakir, M., Huang, Y., et al. (2016). A hyperaccumulation pathway to three-dimensional hierarchical porous nanocomposites for highly robust high-power electrodes. Nat. Commun. *7*, 13432.

ISCI, Volume *19*

Supplemental Information

Ultra-high Areal Capacity Realized in Three-Dimensional Holey Graphene/SnO_2 Composite Anodes

Junfei Liang, Hongtao Sun, Zipeng Zhao, Yiliu Wang, Zhiying Feng, Jian Zhu, Lin Guo, Yu Huang, and Xiangfeng Duan

Supplemental Figures

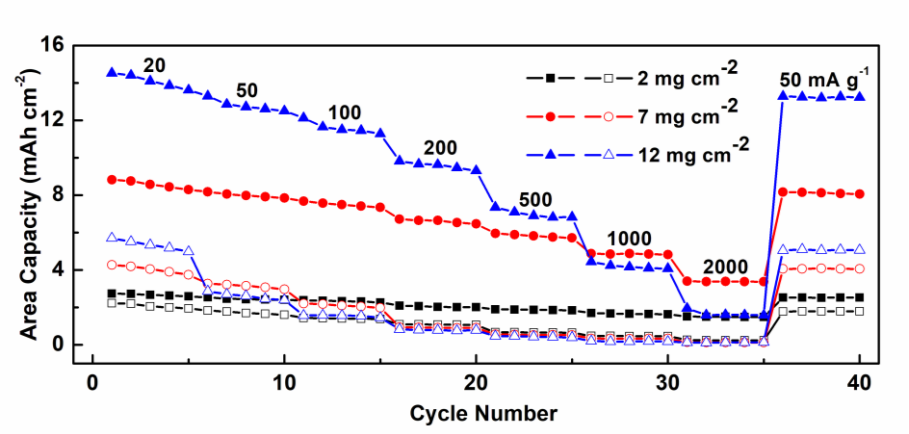

Figure S1, related to Figure 2C. Comparison of the area capacity between 20 mA g^{-1} and 2000 mA g^{-1} for SnO_2/HGF (solid) and SnO_2/G (open) electrodes under different mass loadings (2, 7, and 12 mg cm^{-2}).

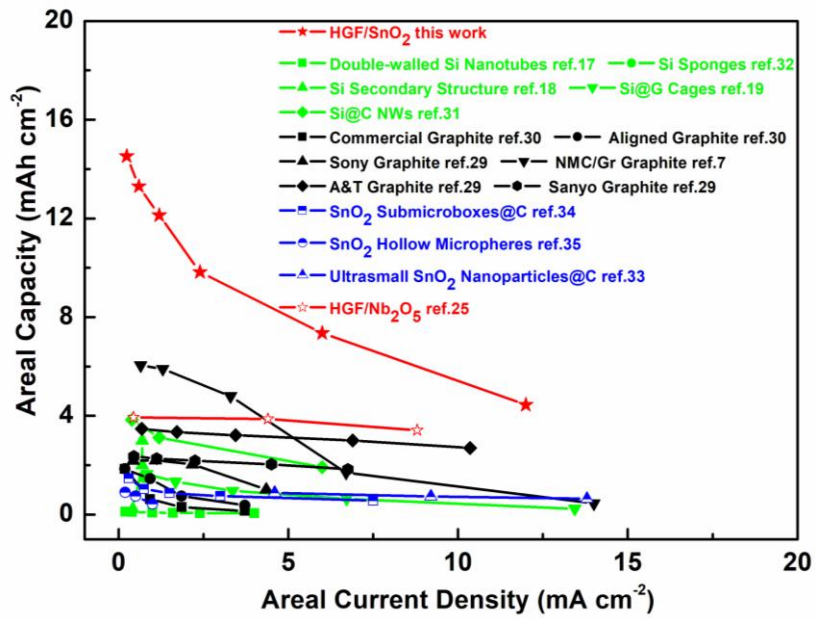

Figure S2. The linear plot of the areal capacity versus current density, related to Figure 4A.

Transparent Methods

Materials: In this study, all the chemicals (purchased from Sigma-Aldrich) were of analytical grade and without further purification.

Synthesis of SnO_2/HGO composite: Graphene oxide (GO) was prepared by oxidation of natural graphite flakes (100 mesh; Sigma-Aldrich) following a modified Hummers' method, and the solution-processable holey graphene oxide (HGO) was synthesized using a previously reported approach (Xu et al., 2015). Briefly, 5 mL of 30% H_2O_2 aqueous solution was mixed with 50 mL of 2 mg mL^{-1} GO aqueous dispersion and then heated at 100 °C under stirring for 2.0 hours. The as-prepared HGO was purified by centrifuging and washing to remove the residual H_2O_2 and then re-dispersed in deionized (D.I.) water. The HGO along with pristine GO sheets were used as building blocks for the synthesis steps described below.

The 3D HGF/SnO_2 composites were prepared using a two-step process. First, using $SnCl_2$ as precursor for SnO_2, SnO_2/graphene composite was prepared in the mixture of water and ethanol by hydrothermal method at 120°C for 12 hours. The intermediate product was centrifuged and washed five times to remove excess ions and then freeze-dried. The product was then annealed at 500°C under argon flow for two hours. The resulting powder sample (SnO_2/G) was dispersed into HGO with magnetic stirring. Excess sodium ascorbate was added into this aqueous mixture and heated at 100°C for 2 hours to reduce the composites. The as-prepared 3D HGF/SnO_2 composites were washed by D.I. water for six times to remove any impurities and cut into thin slices. After freeze-drying, the samples were annealed at 500°C under argon flow for two hours.

Synthesis of control SnO_2/G composites: SnO_2 and graphene powder materials (G/SnO_2) were prepared using the same amount of SnO_2 precursor and GO. The same two-step process was utilized until the G/SnO_2 powder obtained in the step one was well dispersed in GO solution. This solution was freeze-dried and annealed. The resulting G/SnO_2 powders were then used to prepare slurries for battery electrodes.

Material Characterization: The morphology and structure of materials were characterized by scanning electron microscopy (SEM, Zeiss Supra 40VP), transmission electron microscopy (TEM, Titan S/TEM FEI), X-ray diffraction (XRD) (Panalytical X'Pert Pro X-ray Powder Diffractometer). Raman spectra were recorded on a RM 2000 Microscopic confocal Raman spectrometer (Horiba LABHR) using a 488 nm laser beam. Thermogravimetric analysis (TGA, PerkinElmer instruments Pyris Diamond TG/DTA) was conducted in air atmosphere from room temperature to 800°C at a heating rate of 6°C min^{-1}.

Electrochemical Characterization: The free-standing, 3D HGF/SnO_2 electrode composites were mechanically compressed and assembled into coin cells. These electrodes served as the working electrodes without any binders or conductive additives. The control electrode (G/SnO_2) was prepared by mixing 80 wt% active materials, 10 wt% carbon black and 10 wt% polyvinylidene fluoride (PVDF) binder dissolved in N-methyl-2-pyrrolidinone. After the above mixture was coated on Cu foils, electrodes were dried at 120°C under vacuum for 12 h to remove the solvent, and then punched into a disk and pressed. The electrochemical properties were carried out by assembling 2025 coin cells in an argon filled glove box with water and oxygen content kept below 0.1 ppm. Lithium hexafluorophosphate ($LiPF_6$) dissolved in a mixture of ethylene carbonate (EC) and dimethyl carbonate (DMC) was used as the electrolyte (1.0 M $LiPF_6$ in EC/DMC, 1:1 volume ratio, BASF, USA). The typical areal mass loadings of the electrode materials are 2, 7, and 12 mg cm^{-2} for the studies of mass loading dependence. For every electrode with the same mass loading, five cells were tested to determine the data. The tap density of the electrode is around 1.2 g cm^{-3}. The half-cell tests were carried out using Li metal as counter and reference electrode and SnO_2 based composites as the working electrode. Galvanostatic charge/discharge cycling was conducted in a multichannel battery testing system (LAND CT2001A).

Supplemental References

Xu, Y., Chen, C. –Y., Zhao, Z., Lin, Z., Lee, C., Xu, X., Wang, C., Huang, Y., Shakir, M. I., and Duan, X. (2015). Solution processable holey graphene oxide and its derived macrostructures for high-performance supercapacitors. Nano Lett. *15,* 4605–4610.